Thermal Stress Cracking of Slide-Gate Plates in Steel Continuous Casting

HYOUNG-JUN LEE, BRIAN G. THOMAS, and SEON-HYO KIM

The slide-gate plates in a cassette assembly control the steel flow through the tundish nozzle, and may experience through-thickness cracks, caused by thermal expansion and/or mechanical constraint, leading to air aspiration and safety concerns. Different mechanisms for common and rare crack formation are investigated with the aid of a three-dimensional finite-element model of thermal mechanical behavior of the slide-gate plate assembly during bolt pretensioning, preheating, tundish filling, casting, and cooling stages. The model was validated with previous plant temperature measurements of a ladle plate during preheating and casting, and then applied to a typical tundish-nozzle slide-gate assembly. The formation mechanisms of different types of cracks in the slide-gate plates are investigated using the model and evaluated with actual slide-gate plates at POSCO. Common through-thickness radial cracks, found in every plate, are caused during casting by high tensile stress on the outside surfaces of the plates, due to internal thermal expansion. In the upper plate, these cracks may also arise during preheating or tundish filling. Excessive bolt tightening, combined with thermal expansion during casting may cause rare radial cracks in the upper and lower plates. Rare radial and transverse cracks in middle plate appear to be caused during tundish filling by impingement of molten steel on the middle of the middle plate that generates tensile stress in the surrounding refractory. The mechanical properties of the refractory, the bolt tightening conditions, and the cassette/plate design are all important to service life.

DOI: 10.1007/s11663-015-0582-9

I. INTRODUCTION

MOLTEN steel flow from the tundish into the continuous-casting mold is often controlled by an assembly of three refractory plates located between the upper tundish nozzle (UTN) and the submerged entry nozzle (SEN), as shown in Figure 1.[1] The middle plate is connected to a hydraulic cylinder and moves horizontally to adjust the size of the eye-shaped opening to control the flow rate through the nozzle to maintain a constant meniscus level in the mold, according to feedback from the measured level, such as from an eddy current sensor suspended above the mold. Cracking of the slide-gate refractories is an important problem because it poses a great potential safety hazard, in addition to steel quality problems. Even if cracks are rare, discarding slide-gate plates because of the precautionary lifetime limits imposed to avoid potential problems may be very costly.[2] Furthermore, through-thickness cracks may lead to inclusion problems in the steel, due to re-oxidation from air aspiration through the cracks.

Through-thickness radial cracks are a common problem, such as shown in the slide-gate plates in Figure 2(a). Their direction is transverse, either directly perpendicular to the longitudinal axis (lower crack) or angled (upper crack). These cracks are found in almost 100 pct of slide-gate plates, so are referred to as "common cracks". Figures 2(b) and (c) show close-ups of a common crack. The white, inverted triangular-shaped area circled in red on the fracture surface of the through-thickness crack in Figure 2(c) indicates that graphite in the slide-gate plate has been oxidized. This suggests that the steel was likely oxidized as well, producing inclusions or clogging. Figure 2(d) illustrates the location of less common longitudinal and transverse cracks.

Previous research has investigated refractory composition effects to extend service life and achieve higher productivity.[3,4] The refractory composition of the tundish plates is 85 pct Alumina, 8 pct Graphite, and 7 pct Zirconia.[5] Adding the graphite to the refractory improves thermal shock resistance because of the high thermal conductivity, low thermal expansion, and high strength of carbon-bonded alumina refractories.[6,7] Due to their inherent brittleness, refractories are subject to cracking problems. However, the detailed mechanisms and the relative importance of the different stress sources have received little attention.

HYOUNG-JUN LEE, Graduate Student, and SEON-HYO KIM, Professor, are with the Department of Materials Science and Engineering, Pohang University of Science and Technology, 77 Cheongam-Ro, Nam-Gu, Pohang, Gyeongbuk, 37673, Republic of Korea. Contact e-mail: seonhyo@postech.ac.kr BRIAN G. THOMAS, C. J. Gauthier Professor, is with the Department of Mechanical Science and Engineering, University of Illinois at Urbana-Champaign, 1206 W. Green St., Urbana, IL, 61801.

Manuscript submitted October 15, 2015.
Article published online January 28, 2016.

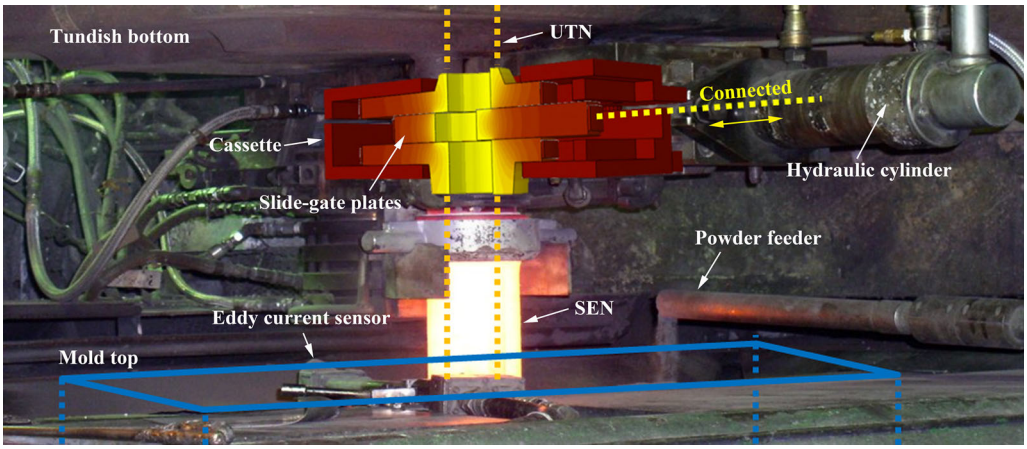

Fig. 1—Slide-gate operation in POSCO plant, Pohang works.

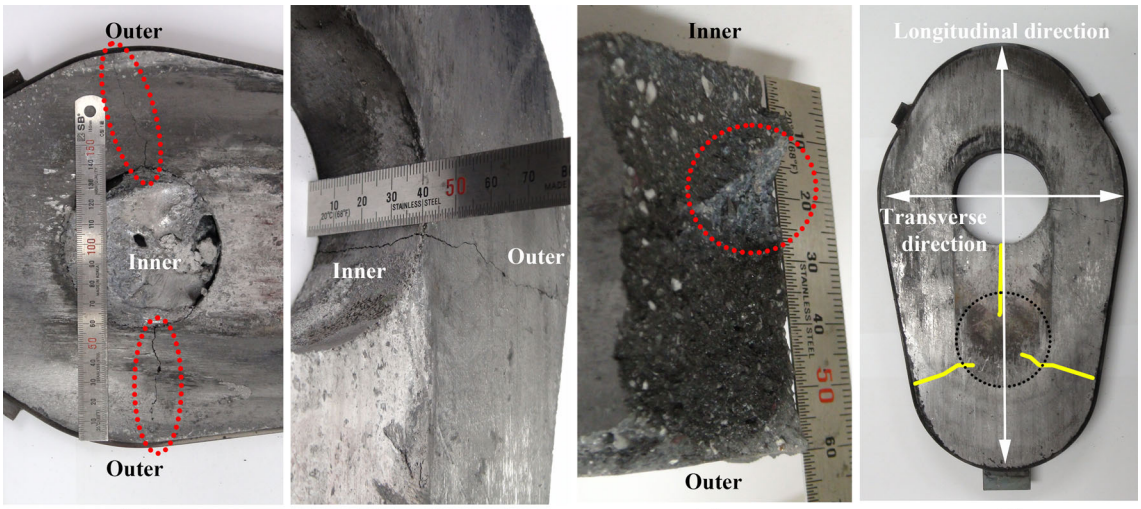

Fig. 2—Type of cracks: (*a*) bottom view of used middle plate and common cracks, (*b*) photo of common through-thickness crack, (*c*) fracture surface of common crack, (*d*) schematic of rare radial/transverse crack locations and the area contacting molten steel during the tundish-filling stage.

When refractories are subjected to high heat transfer and rapid changes in temperature during preheating and casting, the resulting thermal stress may cause cracks.[8] Another source of stress is the mechanical load provided to the plates and cassette by tightening of the bolts, and contact with the guide bumps, which may be non-uniform and create high localized surface pressure. Also, friction forces are generated by the horizontal (back and forth) movements of the middle plate. Finally, ferrostatic pressure due to the height difference between the tundish free surface and slide-gate location provides additional load. In this work, a three-dimensional thermal-stress model was developed and applied to explore thermal and mechanical behavior of a slide-gate plate during preheating, tundish filling, casting[9] and cooling, and to investigate the cracking mechanisms.

II. COMPUTATIONAL MODEL

A. *Heat-Transfer Model*

Temperature, $T(\boldsymbol{x})$, of the components of the slide-gate assembly is found by solving the transient heat-conduction equation:

$$\nabla \cdot (k \nabla T) = \rho C_{\mathrm{p}} \frac{\partial T}{\partial t}, \qquad [1]$$

where k is the thermal conductivity, ρ is density, C_{p} is heat capacity, and $\boldsymbol{x}$ are the three coordinate directions.

Heat convection boundary conditions are applied on the inner and outer surfaces:

$$-k \nabla T \cdot \boldsymbol{n} = h(T - T_{\infty}), \qquad [2]$$

where $\boldsymbol{n}(\boldsymbol{x})$ is the direction normal to the surface, $h(\boldsymbol{x})$ is the convection heat-transfer coefficient, and $T_{\infty}(\boldsymbol{x})$ is

the temperature of the internal or external environment, T_i or T_o: ambient air, preheating gases, or molten steel.

During the preheating stage, internal gas flame temperature and heat-transfer coefficient are needed on the inner surfaces. Based on liquefied natural gas (LNG),[10] containing 88 pct Methane (CH_4), 5 pct Ethane (C_2H_6), 5 pct Propane (C_3H_8), and 2 pct Butane (C_4H_{10}), and stoichiometric air, an ideal flame temperature model[11] gives a gas temperature of 1791 K (1518 °C) with no excess air. However, excess air entrainment consumes some of the heat and prevents direct contact of the flame with the refractory. This was assumed to lower the internal gas temperature to 1023 K (750 °C). The heat-transfer coefficient for forced heat convection from the turbulent flowing combustion products to the contact surfaces on the nozzle interior is found from an empirical equation for smooth cylinders by Petukhov.[12]:

$$\mathrm{Nu} = \frac{[(f/8)\mathrm{Re}\cdot\mathrm{Pr}]}{[1.07 + 12.7(f/8)^{1/2}(\mathrm{Pr}^{2/3} - 1)]}, \qquad [3]$$

where Nu is local Nusselt number (hL/k), Re is Reynolds number ($\rho VL/\mu$), Pr is Prandtl number ($C_p\mu/k$), and f is Darcy friction factor of 0.03.[11] This gives a forced-convection coefficient ($h_{i,\mathrm{preheat}}$) of 65 W/m^2·K.

During preheating, the heat-transfer coefficient for free (natural) convection from the exterior of the cylinder-shaped nozzle to atmosphere is given by the relation for turbulent flow by Churchill et al.[13]:

$$\mathrm{Nu} = \left\{0.825 + \frac{0.387\mathrm{Ra}^{1/6}}{[1 + (0.492/\mathrm{Pr})^{9/16}]^{8/27}}\right\}^2 \qquad [4]$$

$$h = \frac{\mathrm{Nu}\cdot k}{2r}, \qquad [5]$$

where Nu is mean Nusselt number (hL/k), Ra is Rayleigh number ($g\alpha(T_s - T_\infty)L^3/\nu D$), Pr is Prandtl number, h is the free-convection coefficient, k is thermal conductivity, and r is nozzle outside radius, of 0.225 m. This gives a heat-transfer coefficient on the outer surfaces ($h_{o,\mathrm{preheat}}$) of 7 W/m^2·K. Ambient temperatures T_∞ of 373 K and 398 K (100 °C and 125 °C) were measured for preheating and casting stages respectively at the POSCO continuous-casting plant.

During the steel casting stage, the combustion gases are replaced by molten steel, flowing through the slide-gate plate bore at T_∞ of 1823 K (1550 °C). The forced-convection relation for turbulent metal flow from Sleicher and Rouse[14] equation is used:

$$\mathrm{Nu} = 5 + 0.015\mathrm{Re}^{0.88-0.24/(4+\mathrm{Pr})}\mathrm{Pr}^{1/3+0.5\exp(-0.6\mathrm{Pr})} \qquad [6]$$

This gives a heat-transfer coefficient of molten steel ($h_{i,\mathrm{steel}}$) of 28.7 kW/m^2·K.

The heat-transfer boundary conditions of the other slide-gate plate surfaces are from radiation:

$$-k\nabla T\cdot\boldsymbol{n} = q = \varepsilon\sigma_{\mathrm{SB}}\left(T^4 - T_o^4\right), \qquad [7]$$

where q is the temperature-dependent heat flux due to radiation heat loss from the hot plates, ε is the average emissivity of 0.92 for the refractory plates,[15] and 0.75 for the steel cassette,[15] and σ_{SB} is the Stefan–Boltzmann constant, 5.669 × 10^{-8} W/m^2·K^4.

B. *Stress Model*

The mechanical behavior is obtained by solving the following differential equations of force equilibrium:

$$\nabla\cdot\boldsymbol{\sigma} = \boldsymbol{F}, \qquad [8]$$

where $\boldsymbol{F}$ is the force vector from thermal, mechanical, ferrostatic pressure, and bolt loads, $\boldsymbol{\sigma}(\boldsymbol{x})$ is the Cauchy stress tensor, computed from Hooke's law of elasticity:

$$\boldsymbol{\sigma} = \boldsymbol{C} : \boldsymbol{\varepsilon}^{\mathrm{el}}, \qquad [9]$$

where $\boldsymbol{C}$ is the fourth-order tensor containing 81 elastic coefficients:

$$\boldsymbol{C}_{ijkl} = \frac{E}{2(1+\nu)}\left(\delta_{ik}\delta_{jl} + \delta_{il}\delta_{jk}\right) + \frac{\nu E}{(1+\nu)(1-2\nu)}\delta_{ij}\delta_{kl}, \qquad [10]$$

where E is Young's modulus, 65 GPa for refractory, and 206 GPa for the steel cassette[16]; ν is Poisson's ratio, 0.2 for refractory, and 0.3 for steel cassette[16]; and δ_{ij} is Kronecker delta. The elastic strain tensor $\boldsymbol{\varepsilon}^{\mathrm{el}}(\boldsymbol{x})$ is computed from the additive decomposition of the strains:

$$\boldsymbol{\varepsilon}^{\mathrm{el}} = \boldsymbol{\varepsilon} - \boldsymbol{\varepsilon}^{\mathrm{th}}, \qquad [11]$$

where $\boldsymbol{\varepsilon}(\boldsymbol{x})$ is the total strain tensor, computed from the gradient of the displacement field $\boldsymbol{u}(\boldsymbol{x})$:

$$\boldsymbol{\varepsilon} = \frac{1}{2}\left(\nabla\boldsymbol{u} + (\nabla\boldsymbol{u})^T\right) \qquad [12]$$

and $\boldsymbol{\varepsilon}^{\mathrm{th}}(\boldsymbol{x})$ is the thermal strain tensor, calculated from the coefficient of thermal expansion α, the results from the heat-transfer model, $T(\boldsymbol{x})$, and the reference temperature T_0:

$$\boldsymbol{\varepsilon}^{\mathrm{th}} = \alpha(T - T_0)\boldsymbol{I}, \qquad [13]$$

where $\boldsymbol{I} = \delta_{ij}$ is the second-order identity tensor, α is the thermal expansion coefficient, which ranges from 7.03 × 10^{-6} K^{-1} at 298 K (25 °C) to 9.96 × 10^{-6} K^{-1} at 1773 K (1500 °C) with a reference temperature of 1273 K (1000 °C) for this refractory,[16] and is 17.8 × 10^{-6} K^{-1} for the steel cassette.[16]

For this minimally-constrained mechanical system, most boundary surfaces are simply stress free. Mechanical loading is applied indirectly by constraining the horizontal (normal) displacements to zero on those portions of the refractory plate surfaces that touch the guide bumps of the cassette. Additional mechanical loading pressure in the vertical direction is provided by pretension in the four bolts through the cassette, where they contact the upper and lower

plates. The axial tensile force generated in each bolt by tightening is[17]:

$$F_{\text{bolt}} = \frac{2\tau}{d}\left(\frac{\pi d - \mu\lambda}{\lambda + \pi\mu d}\right), \quad [14]$$

where μ is bolt friction, 0.3, λ is bolt thread pitch, 1.5 mm, τ is the bolt tightening torque typically used in the plant, 100 N-m, d is bolt diameter, 28 mm. The resulting axial tensile force generated in the bolt for these conditions, F_{bolt}, is 22.41 kN.

The tensile force produces axial tensile stress in the bolt calculated by,[18]

$$\sigma = \frac{F_{\text{bolt}}}{\pi(d/2)^2}, \quad [15]$$

where σ is the resulting stress, 36.40 MPa.

Ferrostatic pressure acts radially on the inside refractory surfaces exposed to the flowing steel:

$$P_f = \rho g h, \quad [16]$$

where ρ is molten steel density, 7020 kg/m^3, g is gravitational acceleration 9.81 m/s^2, and h is height difference between the tundish free surface and the slide-gate location, 1.8 m. The resulting average ferrostatic pressure, P_f, is 0.124 MPa. Relative to the typical stress from thermal expansion, $-E{\cdot}\alpha{\cdot}\Delta T$, which for a typical temperature variation of 1273 K (1000 °C) is around 540 MPa, this ferrostatic pressure is negligible and so was neglected. Finally, rigid body motion was prevented by constraining the X-, Y-, Z-direction displacements on the surfaces of a stud-hole between the bolts in the lower cassette frame which connects the cassette to the tundish bottom.

C. *Numerical Details*

The above equations were solved in two stages using the finite-element method with the commercial software ABAQUS 6.13-2.[19] First, the heat-transfer model is solved for temperature, $T(x,y,z,t)$, using standard three-dimensional wedge-shaped (DC3D6) 6-node brick elements for the slide-gate plates, hexahedral (DC3D8) 8-node brick elements for the steel band, and both the wedge-shaped and the hexahedral elements for the steel cassette. Then, the stress model is solved using wedge-shaped (C3D6) 6-node brick elements for the slide-gate plates, hexahedral (C3D8R) 8-node linear brick elements for the steel band, 2-node linear truss elements (T3D2) for the bolts, and both wedge-shaped 6-node, and hexahedral 8-nodel brick elements for the steel cassette.

The bolt loads from Equation [14] were applied to each bolt truss element as initial tensile forces at the beginning of the simulation, using the bolt-load method (*Pre-tension section and *Cload) in ABAQUS[19] and given, L bolt length, 84 mm, and E bolt elastic modulus, 206 GPa. The axial displacement of the truss elements is constrained to that of the cassette surfaces under the estimated contact region of each head or nut using distributed coupled constraints (*Coupling and *Distributing method in ABAQUS[19]) to spread the load, according to the displacements of a reference node located at the end of the truss element that is also level with the top surface of the upper cassette frame.

The two-stage simulation starts with the complete transient heat-transfer simulation and the temperature results are input to the mechanical stress model. This required about 1 hour of computation time for the heat-transfer model and 11 hours for the mechanical model on a Windows computer with 8-core 1.80 GHz Intel Xeon Processor and 40.0 GB of RAM.

III. MODEL VALIDATION

The heat-transfer model and its boundary conditions are validated with an analytical test problem and with previous temperature measurements conducted during preheating of a ladle-nozzle plate in a steel plant.

A. *Heat-Transfer Model Validation with Analytical Solution*

To evaluate internal consistency and numerical resolution, the model was first applied to solve one-dimensional transient heat conduction through a cylindrical annulus, representing the preheating of a typical nozzle wall. The heat-transfer coefficients are 70 W/m^2·K for the inside (combustion gas) and 20 W/m^2·K for the outside (ambient air) of the annulus. The ambient temperatures for the inside and outside of the annulus and the initial temperature are all 293 K (20 °C). Further details on the model geometry, properties, and constants are given in Figure 3. The current model simulated a wedge-shaped portion (10 deg) of the nozzle wall with a single layer of the same 3-D elements to be used in the final slide-gate assembly simulations. Except for the thin inner and outer boundary surfaces just discussed, and shown in Figure 3 (colored in red) labeled with arrows, all other surfaces are insulated.

The results are compared with those from a simple spreadsheet-based Visual-Basic-Analysis (VBA) modeling tool,[11] that simulates heat transfer in submerged entry nozzles during preheating, casting and cooling down, and was validated previously.[11] The two solutions match very closely, as shown in Figure 4. The

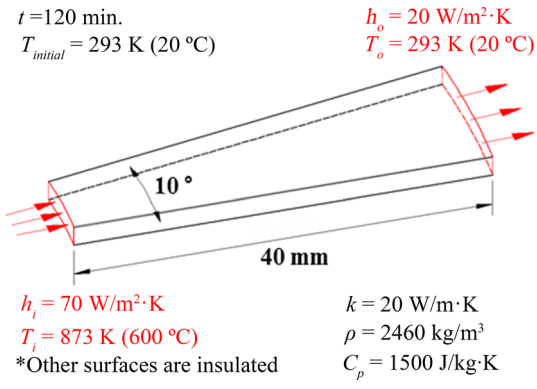

Fig. 3—Schematic of boundary conditions and properties of test problem.

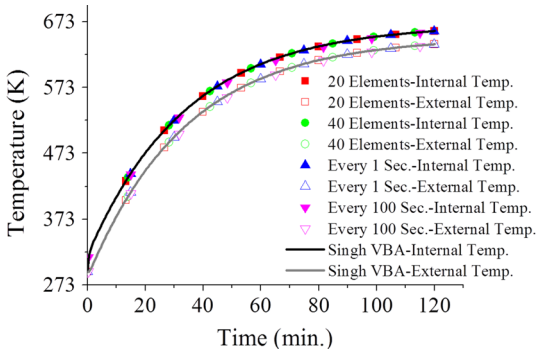

Fig. 4—Temperature history comparison of current model and Singh[11] spreadsheet model.

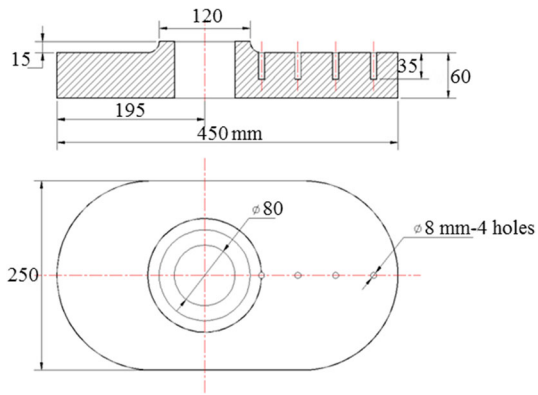

Fig. 5—Geometry of ladle-nozzle slide-gate plate and thermocouple locations.[20]

solutions with 20 and 40 elements also match well, which indicates that 20 elements across the nozzle thickness are sufficient for good spatial resolution. In addition, the solutions with two different time intervals of 1 and 100 seconds are in good agreement, so a time step size of 100 seconds is employed for efficient simulation of the slide-gate nozzle model.

B. *Heat-Transfer Model Validation with Experiments*

To evaluate the choice of heat-transfer boundary conditions, the model was next applied to predict transient 3-D heat conduction in a ladle-nozzle plate, shown in Figure 5. The modeling results were compared with measurements by Simonov et al. made during top teeming of molten steel from a ladle into a tundish.[20] The temperatures were measured with four thermocouples installed in four holes on the non-working top surface of the upper plate, after filling each hole with a solution of magnesite mortar and sintering at 443 K (170 °C). The thermocouples are aligned along the plate symmetry plane to measure temperature variation with distance from the inner bore of the plate.

The mesh of 92,978 wedge-shaped finite elements is shown in Figure 6(a). During the preheating stage, the ladle plate is heated from 298 K (25 °C) to an ambient temperature of 373 K (100 °C) and inside gas temperature of 1023 K (750 °C), followed by steel casting at 1863 K (1590 °C), using the same convection coefficients

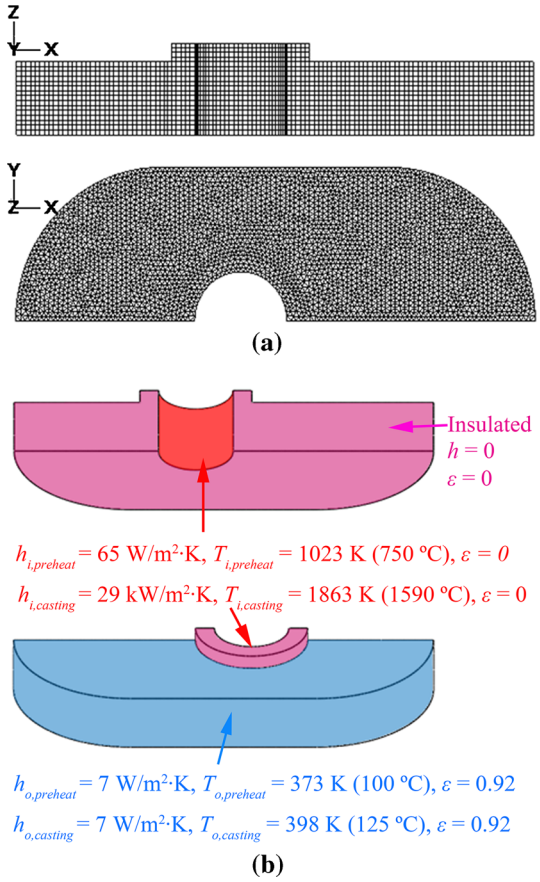

Fig. 6—Heat-transfer model for ladle-nozzle upper plate: (*a*) finite-element model domain and mesh, (*b*) boundary conditions.

as proposed for the tundish-nozzle slide-gate model, and given in Table I. The preheating time was estimated to be 33 minutes, when thermocouple #1 reached 423 K (150 °C). Half of the ladle-nozzle plate is simulated, so the symmetry plane is insulated. The boundary conditions are shown in Figure 6(b). The contact surfaces between the top surface of the upper plate and the upper ladle nozzle, and between the bottom surface of the upper plate and the top surface of the lower plate are also insulated, because the heat exchanged between these surface pairs should be negligible. The thermal properties[16] and constants for this ladle-plate validation problem are given in Table I.

The temperature contours predicted in the upper ladle plate after 73 minutes are shown in Figure 7. The temperature of the ladle plate decreases radially from the plate inner bore to the outside surface with a large, nonlinear temperature gradient due to the large heat capacity of the refractory. Both the experimentally-measured and predicted temperature histories at the four locations of the thermocouples in the ladle plate are compared in Figure 8.

During the 40 minutes of casting, temperatures in the plate were recorded using 7 embedded thermocouples (experiments a and b). The experimentally-measured temperatures and those predicted by the model simulation in the ladle plate match well, especially near the middle of the plate, thermocouples #2 and #3. This suggests that the

Table I. Properties and Constants for Ladle-Nozzle Slide-Gate Validation Problem

	Property or Constant		Value	
	initial nozzle temperature	T_{initial}	298 (25)	K (°C)
Preheating	internal gas temperature	$T_{i,\text{preheat}}$	1023 (750)	K (°C)
	internal convection heat-transfer coefficient (forced)	$h_{i,\text{preheat}}$	65.24	W/m^2·K
	external ambient temperature	$T_{o,\text{preheat}}$	373 (100)	K (°C)
	external convection heat-transfer coefficient (free)	$h_{o,\text{preheat}}$	7	W/m^2·K
Casting	molten steel temperature	$T_{i,\text{casting}}$	1863 (1590)	K (°C)
	internal convection heat-transfer coefficient (forced)	$h_{i,\text{casting}}$	28,720	W/m^2·K
	external ambient temperature	$T_{o,\text{casting}}$	398 (125)	K (°C)
	external convection heat-transfer coefficient (free)	$h_{o,\text{casting}}$	7	W/m^2·K
	density	ρ	3200	kg/m^3
	thermal conductivity	k	8.26	W/m·K
	specific heat	C_p	1004.64	J/kg·K
	Stefan–Boltzmann constant	σ	5.669×10^{-8}	W/m^2·K^4
	emissivity	ε	0.92	–

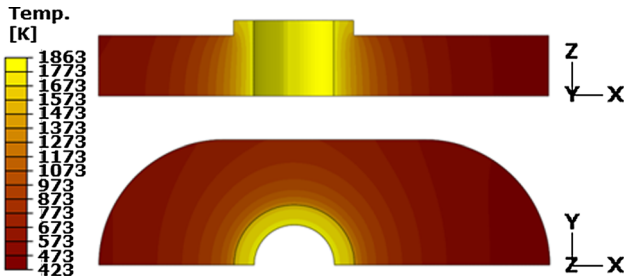

Fig. 7—Ladle plate temperature contours after 73 min of preheating and casting.

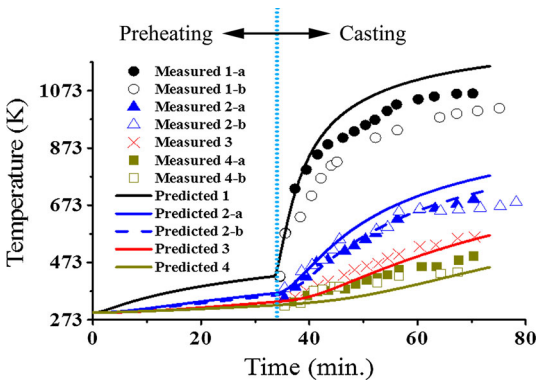

Fig. 8—Comparison of measured[20] and predicted temperature in ladle plate.

assumed internal gas temperature of 1023 K (750 °C) during preheating, and the adopted heat-transfer coefficients are reasonable. Therefore those values were also used for the tundish-nozzle slide-gate simulation.

IV. APPLICATION TO TUNDISH-NOZZLE SLIDE-GATE SYSTEM

A. *Model Details*

A symmetrical half of the tundish-nozzle slide-gate assembly simulated in this work is shown in Figure 9. The upper and lower cassette frames and three slide-gate plates are all clamped together by four bolts. Each of the plates is tightened with a steel band and restrained by contact with the cassette at two guide bumps on each half plate. The middle plate moves back and forth between the guide bumps *via* its connection to a hydraulic cylinder that controls the molten steel flow. Details of the finite-element mesh are shown in Figure 10 and Table II. Two cassette frames, three plates, and three steel bands are modeled with 100,238 elements. Initial loads in the bolts connecting the outer surfaces of the two cassettes were chosen as 22.41 kN, while the contact surfaces between the cassette guide bumps and steel bands and between the plates and steel bands were all assumed to touch with no preload at the initial ambient temperature of 298 K (25 °C).

The material properties and physical constants for both models are shown in Table III. The parameters and boundary conditions of the tundish-nozzle slide-gate model are described in Table IV, for the preheating, tundish filling, casting, and cooling stages, which also contain the boundary conditions at the nozzle inner bore surfaces, and cassette outer surfaces. All other surfaces are insulated. The gap conductance between plates is 0 W/m·K and between the plate and its steel band is 7 W/m·K. For the stress model simulation, the friction coefficient, μ, for the surface to surface contact areas between plates, between steel band and cassette (guide bumps), and between plate and cassette are taken as 0.1,[16] 0.3,[21] and 0.45,[16] respectively.

Starting from ambient temperature with preload, all of the parts are preheated to 1023 K (750 °C) and held for 3.5 hours at the 100 pct (fully opened) position. Then, the middle plate is moved to zero pct opening at 25 mm/s, taking 4.8 seconds, and held for 12.5 minutes while molten steel fills up the tundish. Then, the middle plate is moved to increase the opening to 60 pct, for steady casting. The multiple small movements of that middle plate which occur continuously during the actual process are neglected in the simulation. After 3.5 hours of continuous casting, the opening is moved back to zero pct, and temperature is decreased down to room

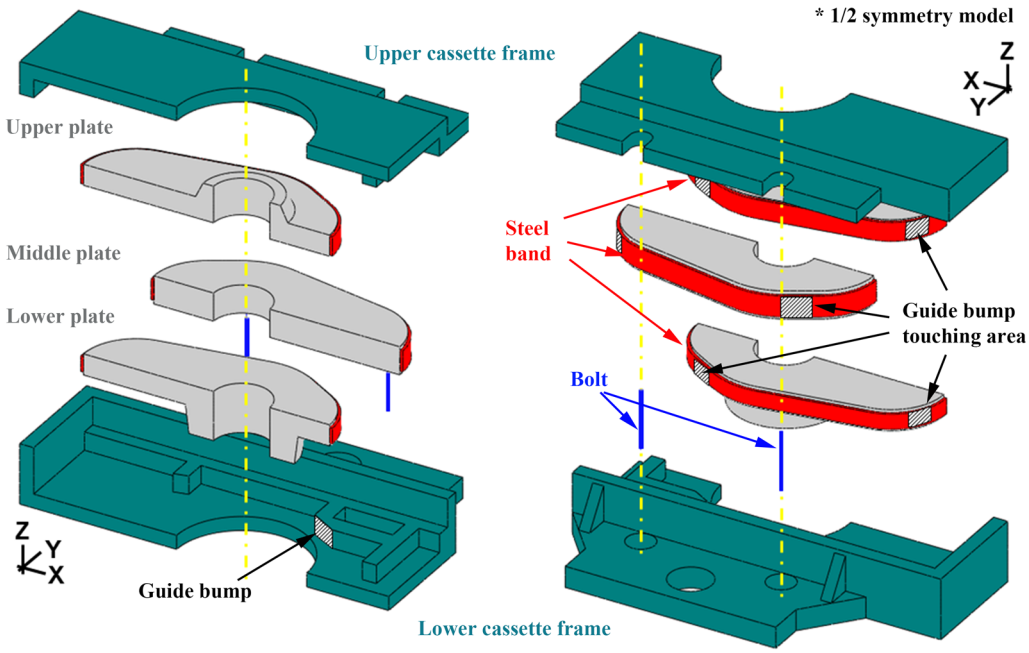

Fig. 9—Exploded view of tundish-nozzle slide-gate assembly.

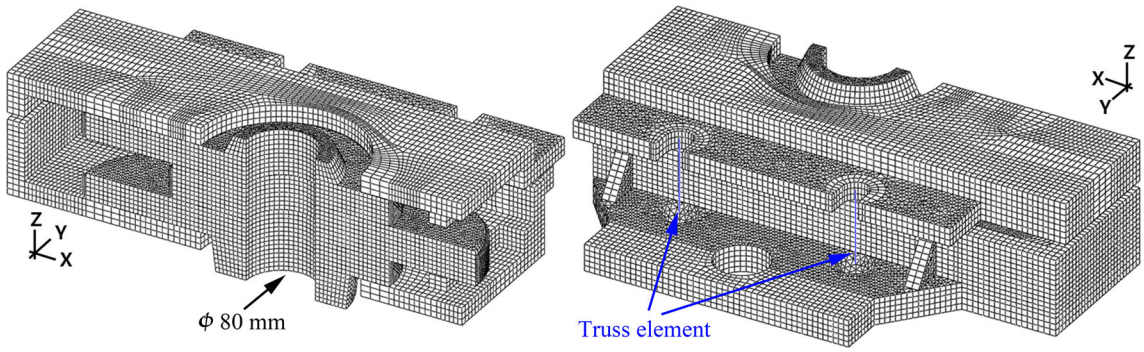

Fig. 10—Finite-element mesh of tundish-nozzle slide-gate assembly.

Table II. Finite-Element Mesh Details for Tundish-Nozzle Slide-Gate Model

	Element Type		
Parts	Hexahedral	Wedge	Truss
Upper plate	–	14,122	–
Middle plate	–	17,016	–
Lower plate	–	18,122	–
Upper band	6356	–	–
Middle band	6750	–	–
Lower band	4972	–	–
Upper cassette	7369	3426	–
Lower cassette	13,965	8138	–
Bolts	–	–	2
Total			100,238

temperature for 4.5 hours. For safety and product quality concerns, the slide-gate nozzle is replaced every 3.5 hours of operation. After running the heat-transfer model for all of these processing steps, the stress model simulation is performed.

B. *Results*

Figures 11(a) and (b) show contours of temperature and stress at the end of the preheating and casting stages, respectively. Temperature in the plates increases

Table III. Properties for Tundish-Nozzle Slide-Gate Model

	Property		Value	
Refractory (plate)	density	ρ_{ref}	3200	kg/m^3
	elastic modulus	E_{ref}	65	GPa
	Poisson's ratio	ν_{ref}	0.2	–
	thermal conductivity	k_{ref}	8.26	W/m·K
	specific heat	$C_{p,ref}$	1004.64	J/kg·K
	expansion coefficient	α_{ref}	7.03×10^{-6}	K^{-1}
	emissivity	ε_{ref}	0.92	–
Steel (band, cassette)	density	ρ_{steel}	7860	kg/m^3
	elastic modulus	E_{steel}	206	GPa
	Poisson's ratio	ν_{steel}	0.3	–
	thermal conductivity	k_{steel}	48.6	W/m·K
	specific heat	$C_{p,steel}$	418.6	J/kg·K
	expansion coefficient	α_{steel}	17.8×10^{-6}	K^{-1}
	emissivity	ε_{steel}	0.75	–
	Stefan–Boltzmann constant	σ	5.669×10^{-8}	W/m^2·K^4

Table IV. Parameters and Boundary Conditions for Tundish-Nozzle Slide-Gate Model

		Preheating	Tundish Filling	Casting	Cooling	
Opening ratio	–	100	0	60	0	pct
Time duration	t	210	12.5	210	270	min.
Initial temperature	$T_{initial}$	298 (25)	–	–	–	K (°C)
Internal sink temperature	T_i	1023 (750) gas	1823 (1550) molten steel	1823 (1550) molten steel	298 (25)	K (°C)
Convection heat-transfer coefficient	$h_{i,forced}$	65	29×10^3	29×10^3	–	W/m^2·K
	$h_{o,free}$	7	7	7	7	W/m^2·K
External ambient temperature	$T_{o,in}$	473 (200)	543 (270)	543 (270)	298 (25)	K (°C)
	$T_{o,out}$	373 (100)	398 (125)	398 (125)	298 (25)	K (°C)

sharply towards the inner bore in the radial direction, especially during casting, when the temperature differences between inside and outside are the greatest. This generates great thermal expansion near the plate bore, which is constrained by the smaller expansion of the cooler outside of the plate. This results in large compressive hoop stress near the inner bore, which is balanced by the simultaneous tension hoop stress towards the outside. At the same time, the general expansion of the plate pushes against the guide bumps, creating radial compression localized in the refractory beneath the steel band, and extra tensile hoop stress localized at the exterior edges of the refractory surface just above and below those guide bumps.

Top views of the middle plate show the predicted temperature contours, Figure 12(a), and corresponding principal stresses, Figure 12(b), after 90 minutes of casting. This figure shows clearly that the two locations of maximum tensile stress on the plate exterior match with the two locations where the observed common through-thickness radial cracks (also in Figure 2(a)) initiate. These results suggest the mechanism of formation for this type of crack. Thermal expansion during heating induces compression near the inner bore, which is balanced by tension in the exterior of the refractory plate. When combined with the pressure at the guide bumps, the maximum principal hoop stress in the center plane is found at the edge of the outer surface near the widest part of the plate. Either of the tensile peaks on the plate surface near the guide bumps, or near the widest part, may initiate cracks which then propagate inwards, from the cold outside surface towards the inner bore.

Mechanical property data such as fracture toughness and tensile strength were not available for this refractory. This is because tensile tests are difficult in brittle ceramics, due to inconsistent surface machining and misalignment during tightening the grips.[3,22] Previous literature[3,23–25] estimates that tensile strength is about 5 to 20 pct of the compressive strength in refractory materials. Based on the measured compressive strength of 245 MPa[5] for this refractory, the tensile strength of the tundish-nozzle slide-gate plates is estimated to range from 12 to 50 MPa.

The bending effect induced on the refractory plates by tightening the bolts is important. The distorted shape of the entire assembly is shown in Figure 13. The squeezing of the cassette causes its outer frame to pivot around the sharp edges of the plate, in both the X- and Y-directions, resulting in large gaps and high localized stresses in the plates. The largest gap of 0.188 mm forms between the upper cassette frame and the upper refractory plate, as shown in Figure 13(b). As shown in Figures 13(c) and (d), the bending causes tensile stress at the outer plate surface edge (nearest the pivot points), with localized compressive stress regions in the interior of the plates.

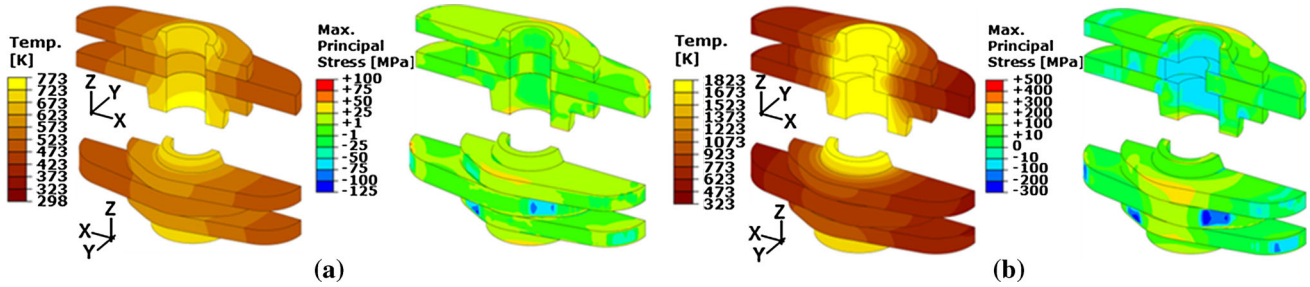

Fig. 11—Temperature and maximum principal stress contour snapshots in the refractory at the end of: (*a*) preheating (after 3.5 h), (*b*) continuous casting (after 3.5 h).

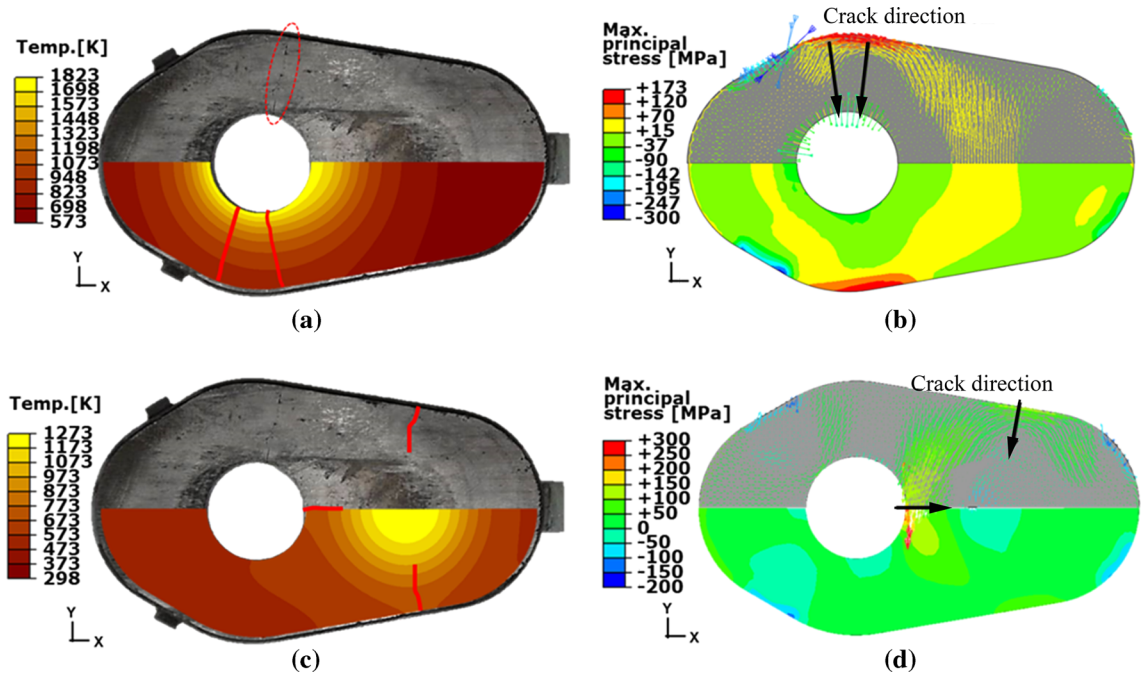

Fig. 12—Crack formation mechanisms comparing photographs of used plates, temperature contours, and stress distribution (direction and magnitude in center section view) showing where cracks initiate and grow: (*a*, *b*) common through-thickness radial crack formation in the middle plate during casting (after 90 min), (*c*, *d*) rare radial and transverse crack formation in the middle plate during tundish filling (after 5.5 min).

Predicted temperature and stress histories at critical locations on the plate surface are shown in Figure 14, during the preheating, tundish filling, casting and cooling stages. Lines and dots show stress histories with and without bolt preload, respectively. In all three plates, the stress shown at location 1 is the maximum principal hoop stress perpendicular to the growth direction of common through-thickness cracks. The stress at location 2 in the upper and lower plate, and at location 4 in the middle plate, is the Y-direction stress important for the rare radial cracks. The stress at location 3 in the middle plate is in the tangential (~X) direction along the outside edge of the plate important for the transverse cracks.

At time zero, after applying only the bolt preload, Figure 14(d) shows that the initial principal stresses in the middle plate does not exceed the tensile strength of 12 to 50 MPa anywhere. Thus, cracks in the middle plate are not caused by the bolt loads, unless a piece of sand or grit gets trapped between the plates. However, the bending of the cassette frame about the X axis caused by the initial bolt loading causes high tensile Y-stress at location 2 (rare radial crack location) along the center line of the top surface of the upper plate, and the bottom surface of the lower plate, as shown in Figures 14(b) and (f). This might initiate rare radial cracks in the upper and lower plates along the X–Z symmetry plane, perpendicular to the Y-stress direction during preheating, tundish filling or casting, when the hot gases or molten steel heat the nozzle bore.

During the first 10 minutes of preheating, Figure 14(b) shows that the principal tensile stresses increase into the tensile-strength range at location 1 in the upper plate, where common through-thickness radial cracks are observed to initiate. Thus, common through-thickness radial cracks are likely to form during preheating due to tension induced by thermal expansion of the bore. This cracking time is consistent with observations by steel plant engineers.[2]

During the first few minutes of tundish filling, the hot molten steel heats the nozzle bore and the expansion

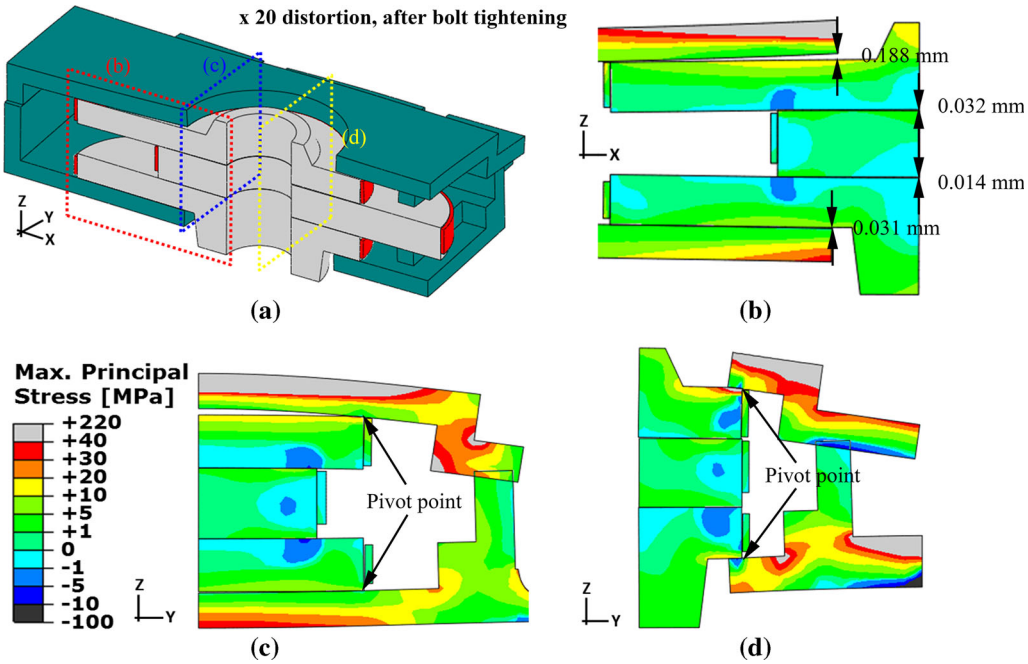

Fig. 13—Distorted shape of bolted cassette and slide-gate assembly after bolt loading (zero time, 20 times magnification): (*a*) isometric view of distorted assembly showing locations of cross-sectional views showing maximum principal stress contours, (*b*) in X–Z symmetry plane with gap distances between mating surfaces, (*c*) in Y–Z plane at inner bore edge, (*d*) in Y–Z plane at inner bore center.

generates even higher tension in the outer surface of the upper plate (blue line in Figure 14(b)). This always exceeds the tensile-strength range at the exterior edges to cause common through-thickness radial cracks in every upper plate, if they had not already formed during preheating. In addition, a round area on top of the middle plate is contacted by the molten steel to become very hot and highly compressed (Figure 2(d)). This compression generates tension in the inner bore (location 4), as shown in Figure 14(d). This mechanism may initiate rare radial cracks that propagate outward along the X–Z symmetry plane, perpendicular to this tensile stress (Figures 2(d) and 12(c)).

The compression in the hot circular contact area also generates a tension hoop stress in the surrounding refractory, as shown in Figures 12(c) and (d). This includes the nearest surface at location 3, where ~X-tensile stress during tundish filling exceeds the refractory strength (Figure 14(d)). Thus, rare transverse cracks could initiate at the outside surface (location 3) and propagate inward during tundish filling. This mechanism could explain the formation of transverse cracks in the middle plate. The lower plate is not influenced by the molten steel during this filling stage (zero pct opening).

During the casting stage, the general heating of the entire assembly causes thermal expansion that generates high localized compression in the guide bump region of all 3 plates. In addition, the general expansion greatly increases the bending stresses induced from the bolted cassette, which causes the Y-tension at location 2 in Figure 14 to increase greatly in the outside surfaces of the upper and lower plates. This causes a chance for rare radial cracks in the upper and lower plates.

The mechanism of rare radial cracks in upper and lower plate is tension in the Y-direction caused by bending from the bolt preload combined with the greatest thermal expansion of the plates during casting. Thus, increasing bolt preload on the cassette assembly exacerbates rare radial cracks through the upper and lower plates.

Also during casting, the greatest temperature differences between inside and outside cause the hoop-direction tension at location 1 to become the largest during this time in all three plates. This gives another chance to initiate rare and common through-thickness radial cracks near location 1, if they had not formed already during preheating and tundish filling.

During the final cooling stage, the hottest area, which is the inner bore of the plates in contact with molten steel during casting, cools down to ambient temperature. The accompanying thermal contraction of the inner bore and nearby surfaces of the middle plate at location 4, combined with much slower cooling of the rest of the plate, generates tensile stress in the Y-direction, as shown in Figures 14(c) and (d). Accordingly, a rare radial crack may initiate and propagate during cooling.

V. CONCLUSIONS

This paper investigates the thermal and mechanical behavior of tundish-nozzle slide-gate assembly during preheating, tundish filling, continuous casting, and cooling down, using a three-dimensional finite-element model. In addition to the three nozzle plates, it is important that the model includes the steel cassette frame and the bolts which hold the assembly together. The heat-transfer model and its boundary conditions are validated with an analytical test problem, and with previous experimental temperature measurements of a

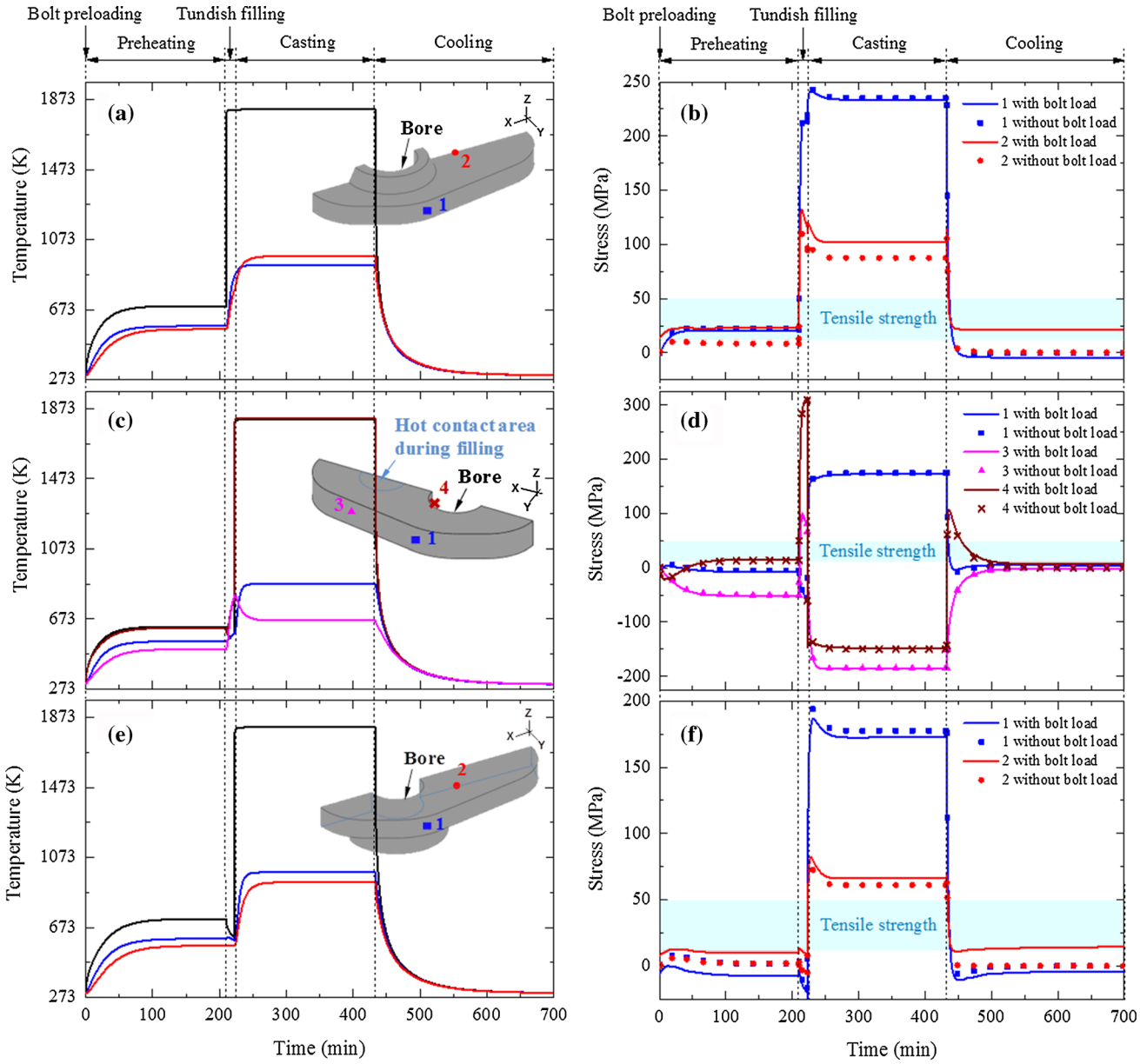

Fig. 14—Predicted temperature histories and stresses in tangential (~X) direction (1 = blue, 3 = purple) and Y-direction (2 = red, 4 = brown) at critical surface locations, during preheating, tundish filling, casting, and cooling: (*a*, *b*) upper plate, (*c*, *d*) middle plate, (*e*, *f*) lower plate.

ladle-nozzle slide-gate plate. Results for the steel continuous-casting process suggest different mechanisms for different types of cracks:

The common through-thickness radial cracks in all three plates (location 1): Thermal expansion due to radial temperature variations through the plate is the most important mechanism causing common through-thickness radial cracks in almost every plate in commercial practice. During the early stages of preheating or during tundish filling, heating of the nozzle bore from the hot gases or molten steel causes internal compression that generates tensile stress at the outer surface of the plate. When combined with the pressure at the guide bumps, the maximum principal hoop stress is generated in the widest part of the plate, which initiates cracks that propagate radially inward. This cracking mechanism might be lessened by improving the fracture toughness of the refractory, removing surface imperfections, especially at the outer surface, or perhaps by tightening the outer steel band to lessen the expansion.

The rare radial cracks in upper and lower plate (location 2): The vertical loads applied to the cassette assembly from tightening the bolts can exacerbate rare radial cracks through the upper and lower plate, due to mechanical bending stresses. These bending stresses increase during casting due to thermal expansion, which generates significant bending tension even without the bolt loads. In general, geometric design of the cassette and plate perimeter shape appears to constrain the plates to apply excessive pressure at the slide-gate plates by bending of the cassette during operation. Therefore this geometry should be optimized to accommodate the

thermal expansion and to avoid excessive bending forces, and bolt tightening also should be optimized (lessened) to prevent rare radial cracks due to excessive bending.

The rare transverse and radial cracks in the middle plate (location 3, 4): Compressive stresses generated during tundish filling in the hot circular contact area, where the hot molten steel impinges on the middle of the middle plate, can cause tensile stresses in the surrounding refractory. This may form rare transverse and radial cracks in the middle plate. The preheating temperature and duration time should be increased to prevent this mechanism.

In addition, as the plates cool down after continuous casting is complete, further tensile stress is generated by thermal contraction of the cooling inner bore. This is another mechanism that may propagate rare radial cracks radially outward from the inner bore. To alleviate this mechanism, slower, more uniform cooling rate is recommended.

To make the model predictions more quantitative, future work is recommended to measure the tensile strength of this refractory material, such as bending tests with varying temperature. In addition, the possible effect of time and residual stress changes caused by creep on these phenomena and cracking mechanisms should be investigated.

ACKNOWLEDGMENTS

The authors wish to thank POSCO (Grant No. 4.0009576.01), the Clean Steel and Nonferrous Metals Processing Laboratory at POSTECH, and the Continuous Casting Consortium at the University of Illinois at Urbana-Champaign for financial support. Thanks are also given to Sang-Woo Han – POSCO Technical Research Laboratories, Sung-Kwang Kim – POSCO Gwangyang Works, and to Kwon-Myung Lee – DOOSAN Heavy Industries for supporting plant data.

REFERENCES

1. J. Choi: *Understanding of Continuous Casting*, POSCO Technical Research Lab, Pohang, 2009.
2. S.K. Kim: POSCO Gwangyang Works, Gwangyang, Jeonnam, Korea, private communication, 2010.
3. W.D. Kingery: *J. Am. Ceram. Soc.*, 1955, vol. 38, pp. 3–15.
4. L.A. Diaz, R. Torrecillas, F. Simonin, and G. Fantozzi: *J. Eur. Ceram. Soc.*, 2008, vol. 28, pp. 2853–58.
5. Properties of Plate Bricks, Chosun refractories Co. Ltd., Pohang, Gyeongbuk, Korea, 2008.
6. H. Liu: *Adv. Mater. Res.*, 2012, vols. 538–541, pp. 660–64.
7. B. Rand, A.S. Ahmed and V.P.S. Ramos: *Proc. of Tehran Int. Conf. on Refract.*, Tehran, Iran, 2004, pp. 40–55.
8. Z.H. Jin and Y.W. Mai: *J. Am. Ceram. Soc.*, 1995, vol. 78, pp. 1873–81.
9. H.J. Lee, S.M. Cho, S.H. Kim, B.G. Thomas, S.W. Han, T.I. Chung and J. Choi: *AISTech Conf. Proc.*, Atlanta, GA, 2012, pp. 1329–38.
10. Fundamentals of Gas, Korea Gas Safety Corporation, Eumseong, Chungbuk, Korea, 2015.
11. V.K. Singh and B.G. Thomas: *Continuous Casting Consortium Annual Report*, University of Illinois at Urbana-Champaign, IL, 2010.
12. B.S. Petukhov: *Adv. Heat Trans.*, 1970, vol. 6, pp. 503–64.
13. S.W. Churchill and H.H.S. Chu: *Int. J. Heat Mass Trans.*, 1975, vol. 18, pp. 1323–29.
14. C.A. Sleicher and M.W. Rouse: *Int. J. Heat Mass Trans.*, 1975, vol. 18, pp. 677–83.
15. Table of Total Emissivity, Omega Engineering Inc., Stamford, CT, 2015.
16. Y.H. Kim and J.M. Sun: Chosun Refractories Co. Ltd. Technology Research Institute, Pohang, Gyeongbuk, Korea, Private Communication, 2010.
17. J.E. Shigley and C.R. Mischke: *Mechanical Engineering Design*, 6th ed., McGraw-Hill, New York, 2001.
18. B.G. Thomas, G. Li, A. Moitra, and D. Habing: *Iron Steel Maker*, 1998, vol. 25, pp. 125–43.
19. Abaqus 6.13-2 Documentation, Dassault Systèmes Simulia Corp., Providence, RI, 2013.
20. K.V. Simonov, S.I. Rabochkin, A.A. Kortel, and L.A. Reinov: *Refract. Ind. Ceram.*, 1979, vol. 20, pp. 742–46.
21. L.C. Hibbeler, B.G. Thomas, R.C. Schimmel, and G. Abbel: *Metall. Mater. Trans. B*, 2012, vol. 43B, pp. 1156–72.
22. T. Andoh and H. Shikano: *Refractories Handbook*, The Technical Association of Refractories, Tokyo, 1998.
23. Experiment-Ceramics, ME3701, Material of Engineering Laboratory, Louisiana State University, LA, 2015.
24. CIP 16-Flexural Strength Concrete, National Ready Mixed Concrete Association, Silver Spring, MD, 2000.
25. S. Pul: *Indian J. Eng. Mater. Sci.*, 2008, vol. 15, pp. 467–72.